Concentration fluctuations in the binary mixture hexane-nitrobenzene with static and dynamic x-ray scattering

Eric M. Dufresne, Teamour Nurushev, Roy Clarke, and Steven B. Dierker*
Department of Physics, University of Michigan, Ann Arbor, Michigan 48109-1120
(Received 10 July 2001; revised manuscript received 3 April 2002; published 21 June 2002)

We report on a small-angle x-ray scattering study of the hexane-nitrobenzene binary fluid mixture near its critical point. The use of an ultrabright x-ray undulator synchrotron source enabled us to measure the temperature dependence of the static structure factor with unprecedented contrast, and the large coherent flux of this source provided a probe for the fluctuation dynamics via the x-ray photon correlation spectroscopy technique. We find that the intensity and correlation lengths diverge with the expected three-dimensional Ising critical exponents, and the dynamical correlation function decays exponentially with correlation times as small as 250 μs. In the range of wave vector studied here ($1.2–2.6\times10^{-3}$ Å^{-1}) the concentration fluctuations relaxed diffusively with a diffusion constant consistent with that determined from visible light scattering measurements.

DOI: 10.1103/PhysRevE.65.061507 PACS number(s): 64.70.Ja, 64.60.Fr, 61.10.Eq, 61.25.Em

I. INTRODUCTION

Due to the large coherent flux of third generation synchrotron sources, the technique of x-ray photon correlation spectroscopy (XPCS) is now performed on an increasing variety of samples [1–9]. In a XPCS experiment, one studies the time correlation function of fluctuations of a speckle pattern [10], which is produced when a beam of coherent x rays is scattered by spatial inhomogeneities in a material. XPCS has the potential to measure the relaxation rate of the dynamic structure factor of materials over a wide range of time scales (1 μs-1000 s) in and out of thermodynamic equilibrium at wave vectors inaccessible to visible light (0.004–2 Å^{-1}). The technique of visible PCS [11] allowed for great advances in our understanding of dynamical critical phenomena. XPCS experiments should expand our understanding of short length scale fluctuations, as well as enable studies of opaque materials such as metal alloys.

Most of the results reported to date have been performed on systems with a large length scale microstructure which greatly enhances the scattered intensity due to the coherent addition of the scattering from the large number of atoms in the microstructure. This includes aggregate systems such as colloids [2,3,6,8,9] and polymer micelles [5], spinodally decomposing systems such as sodium borosilicate glass [12], and systems with antiphase domains such as metal alloys [1,4,13]. Binary mixtures of small molecular weight fluids have much faster fluctuations (μs to s), and they typically scatter more weakly than systems studied previously. As such, they represent an important test of the general applicability of XPCS to a wide variety of materials.

In this paper we report the scattering rate of composition fluctuations in a binary mixture, *n*-hexane (C_6H_{14}) and nitrobenzene ($C_6H_5NO_2$), measured with small angle x-ray scattering (SAXS) on a sample at the critical composition. Although simple binary fluids have been studied extensively by light and neutron scattering techniques [14,15], only one SAXS experiment has been reported on binary fluids and it did not provide a determination of the absolute scattering intensity from composition fluctuations [16]. It is also interesting to point out that due to the extremely small source size of third generation synchrotron sources and their large increase in brilliance over laboratory sources, our experiment was performed with much better resolution than previous work done on a rotating anode source, which was performed with tight collimation in one direction, but no collimation in the other perpendicular direction [16]. The high degree of collimation of our setup simplifies the data analysis considerably.

The mixture of *n*-hexane and nitrobenzene has a relatively high x-ray contrast making it a good choice for XPCS. We report below the XPCS measurements done on a simple binary fluid near its critical point. With a coherent flux of 8.7 keV x rays equal to 3.6×10^{10} photons/s in an aperture of $(5\ \mu\text{m})^2$, we measured scattering rates of about 100–1000 photons/s per speckle for a temperature within 0.06 °C from the critical temperature and with a 3 mm thick sample. We measured dynamic correlation functions with simple exponential decays, the fastest being approximately 250 μs. Our measurements show that it will be feasible to use XPCS to study the dynamics of even such weak scatterers as these low molecular weight hydrocarbon fluid mixtures. This further demonstrates the general applicability of XPCS to a wide variety of materials. The measurements reported only collected and analyzed a single speckle and are limited to wave vectors that are also accessible with visible light scattering. However, with modest amounts of multispeckle signal averaging such as with a fast row-shifting technique using a charge-coupled device (CCD), tests of the dynamics of critical fluctuations at higher wave vector than previously achievable by visible light PCS should be quite feasible. Our results are also noteworthy in that the hexane-nitrobenzene mixtures showed no detectable signs of radiation damage even under the high intensity of a so called ''pink'' undulator beam at a third generation source such as the Advanced Photon Source (APS). This is in contrast to preliminary evidence obtained by us as well as other researchers on colloidal and

*Also at the National Synchrotron Light Source, Brookhaven National Laboratory, Upton, NY 11973.

polymer samples, which are typically quite sensitive to radiation damage or x-ray induced charging effects.

II. THEORY AND DATA ANALYSIS

Binary mixtures are in the same universality class as the three dimensional (3D) Ising model [14–16]. The structure factor for scattering from concentration fluctuations of a binary mixture can be written as

$$S(q,T) \propto k_B T \chi G(q\xi), \tag{1}$$

where $G(x)$ is a scaling function, T the temperature, χ the osmotic compressibility, q the wave vector, and ξ the correlation length of the composition fluctuations [14]. Near the critical point of a continuous phase transition, many physical properties of a system can be expressed as power laws of the reduced temperature $t = T/T_c - 1$, where T_c is the critical temperature.

Previous light scattering measurements on *n*-hexane–nitrobenzene mixtures determined that the correlation length $\xi = \xi_0 t^{-\nu}$, with $\nu = 0.635 \pm 0.005$ and the bare correlation length $\xi_0 = 3.54 \pm 0.15$ Å. The osmotic compressibility is found to scale as $\chi \propto t^{-\gamma}$ with $\gamma = 1.23 \pm 0.01$ [14]. No exact analytical expression is known for $G(x)$ for the 3D Ising universality class [14–16]. We simply model it with an Ornstein-Zernicke form $G(x) = (1 + x^2)^{-1}$. Since in our experiment, $x < 3$, the Ornstein-Zernicke form is more than adequate to model $G(x)$ [15]. Thus the measured scattering intensity, $I(q,T)$, can be written

$$I(q,T) = \frac{I_0 t^{-\gamma}}{1 + q^2 \xi_0^2 t^{-2\nu}} + B(q), \tag{2}$$

where $B(q)$ includes parasitic scattering from other materials in the x-ray beam path and a temperature independent structure factor from each of the individual components of the mixture. Izumi [16] has pointed out the importance of measuring this background carefully by measuring the scattering from each individual component in the sample cell and then modeling the background from the individual components as a weighted average of their individual backgrounds.

Since it is difficult to measure $B(q)$ properly, we chose another approach to model the measured structure factor introduced by Damay *et al.* [15]. We use the scan performed at the highest temperature T_{max} as a rough approximation of a background scan and fit the difference

$$I(q,T) - I(q,T_{max}) = I_0 \left[\frac{t^{-\gamma}}{1 + q^2 \xi_0^2 t^{-2\nu}} - \frac{t_{max}^{-\gamma}}{1 + q^2 \xi_0^2 t_{max}^{-2\nu}} \right], \tag{3}$$

for all the scans with $T < T_{max}$. This approach is sufficient when $B(q)$ is temperature independent and we utilized it in our data analysis. In this fit, the parameters I_0, T_c, ξ_0, ν, and γ are optimized by minimizing the χ^2 of the whole data set. We are able to derive $B(q)$ by subtracting the small critical scattering contribution from the data at T_{max}.

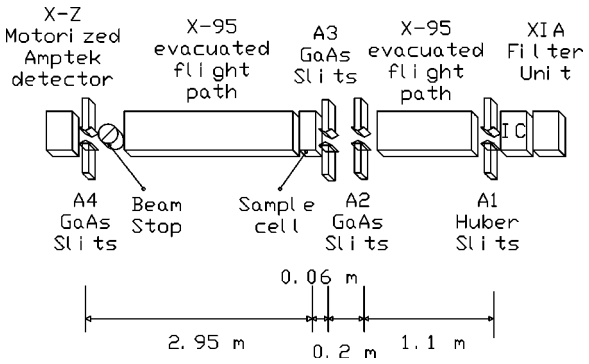

FIG. 1. The experimental setup.

III. EXPERIMENTAL METHOD

A. SAXS experimental setup

This experiment was performed on the undulator beamline at sector 7 of the Advanced Photon Source, operated by MHATT-CAT, the University of Michigan/Howard University/Lucent Technologies-Bell Labs Collaborative Access Team. The fundamental energy of the undulator was set to 11.0 keV. The x-ray beam was incident on a double crystal Si (111) monochromator set to diffract 11.0 keV x rays corresponding to a wavelength $\lambda_0 = 1.1271$ Å, with a bandpass of approximately 0.014%. With an ion chamber, we measured a monochromatic intensity of 7.7×10^{10} photons/s in an aperture of $(100\ \mu\text{m})^2$ incident on the sample for a ring current of 100 mA.

The experimental setup is schematically shown in Fig. 1. We collimated the monochromatic beam in our experimental hutch with two 100 μm$\times$100 μm apertures (A1 and A2 in Fig. 1) defined by slits and separated by approximately 1.1 m. These slits will reject stray parasitic scattering from most of the upstream beamline components in the wave vector range of interest in this experiment. A third guard slit A3 was set to 150 μm$\times$150 μm and placed approximately 20 cm behind aperture A2. The sample was placed 6 cm behind aperture A3.

At the end of this flight path, a stepper motor driven detector stage could move various detectors in a plane perpendicular to the incoming x rays. The scattered x rays were measured with an Amptek XR-100CR detector. This detector has a quantum efficiency $\epsilon = 0.82$ at 11.0 keV. The detector output was amplified by a fast Canberra 2025 amplifier. The detector resolution was defined by another aperture set to 600 μm$\times$600 μm, and placed 2.95 m from the sample. It defined a detector resolution $\Delta q = 2\pi/1.1271$ Å$\times$600 μm/2.95 m$= 1.13 \times 10^{-3}$ Å^{-1}.

The sample was mixed at a critical composition [14] of 41.6 mole % of nitrobenzene by weighing the two components with a precision scale. The sample cell was a 10 mm thick Al cylinder, sealed by two 2 mil Kapton windows. This cell was mounted on an Al block that was temperature controlled by a Lauda closed-loop water bath. The sample temperature, measured with a precision thermistor, was stable to within 20 mK during the duration of a scan. The measured x-ray transmission from the mixture was 35%, which corresponds to 1.05 x-ray absorption lengths. Using data provided

TABLE I. Some physical constant of *n*-hexane and nitrobenzene.

	n-hexane	Nitrobenzene
Chemical formula	C_6H_{14}	$C_6H_5NO_2$
Density (g/cm^3)	0.659	1.196
Molar mass	86.18	123.11
Weight fraction in mixture (%)	49.5	50.5
Z	50	64
Volume per molecule (nm^3)	0.217	0.171
ρ_e (nm^{-3})	230	374.5
δ (cm)	1.14	0.387

in Table I, the mixture's penetration depth, calculated by weighting each component's mass absorption coefficient $(\rho\delta)^{-1}$ with its weight fraction, is 6.7 mm which compares reasonably well to the measured 9.5 mm deduced from the x-ray measurements.

B. XPCS experimental setup

For the XPCS measurements, we set the undulator fundamental at 9.0 keV. The white beam was collimated with white beam slits set to nominally 100 μm by 100 μm and placed 27 m from the source. In the experimental hutch 35 m from the source, two small Pt coated mirrors separated by 0.95 m and set at 0.45° were used to produce a pink beam. These mirrors act as a low pass filter for the white beam. The doubly reflected beam had a spectrum with an average energy of 8.73 keV, with a bandpass of $\Delta E/E=2.55\%$. A coherent x-ray intensity as large as 3.6×10^{10} photon/s in an aperature of $(5\ \mu\text{m})^2$ was incident on the sample. Assuming the spectrum is Lorentzian, one can show that the longitudinal coherence length for this beam is approximately $l_l=0.318\lambda/(\Delta E/E)=17.7$ Å [17,18]. For the XPCS setup, the 1 m long flight path between A1 and A2 in Fig. 1 was replaced by two small UHV mirror tanks separated by a bellow. The aperture A1 was a 0.2 mm diameter hole made in a 1 mm thick Ta foil. The various distances between the apertures are shown in Table II.

The smallest transverse coherence length at the APS is in the horizontal since the horizontal source size is approximately a factor ten times bigger than the vertical size. The coherence length is thus $l_h=\lambda R_e/(2\sqrt{\pi}\sigma_x)$, where $R_e=37$ m is the source-sample distance, and $\sigma_x=300$ μm is the rms horizontal source size [19]. For the pink beam, the transverse coherence length is 4.8 μm, thus aperture A2 was set to 5 μm$\times$5 μm to select a transverse coherent beam. In Appendix A, we show that the longitudinal coherence condition for a pink beam is valid for wave vectors below 1.6×10^{-3} Å^{-1}. For wave vectors above this value, the contrast of the speckle pattern is reduced [4,18]. Given that the relaxation rates for the mixture are increasing quadratically with increasing wave vectors, one is only able to measure sufficient scattering rate per speckle per correlation time near this limiting wave vector, thus the pink beam is very well suited for such a system.

TABLE II. Some useful distances and experimental parameters.

Distances	SAXS setup	XPCS setup
A1-A2 (m)	1.1	2.214
A2–A3 (m)	0.2	0.203
A3–sample	0.06	0.06
Sample–A4	2.95	1.24
Average energy (keV)	11.0	8.73
Speckle size (μm)	60	20

We show in Appendix A that the speckle size in the detector plane is approximately 20 μm. We were able to measure dynamic correlation function on the hexane-nitrobenzene binary mixture with a detector aperture of 20 μm$\times$20 μm, but typically we opened up the detector aperture to improve the signal to noise ratio of the measurement. A Brookhaven Instrument BI-30 hardware correlator was used to measure the dynamical correlation functions. An in-vacuum horizontal 200 μm thick Ta wire acted as a beam stop before the exit Be window of the 1 m long detector flight path.

The sample oven was redesigned for the XPCS experiment. The sample oven is a standard three stage oven, built as an Al cylindrical multilayered enclosure [20]. The outer shell is at room temperature, and surrounds an active shell whose temperature is controlled by a Lauda closed-loop water bath. The inner shell is heated by an electrical element controlled by a Lakeshore DRC-92C controller. The stability of the temperature as read by an independent thermistor was stable to 5–10 mK. The aluminum sample holder is designed as a coin stack of thin cylinders with a large enough sample volume to provide a weigh in mixing for the sample. The thickness of the sample is 3 mm along the beam and terminated by two 5 mil Be windows.

IV. RESULTS

A. SAXS results and absolute cross section

Figure 2 shows the temperature dependence of the measured SAXS scattering rate for the critical composition. As expected, the scattering rate increases as the temperature is lowered toward T_c. The left-right asymmetry in the scattering rate is most likely due to an asymmetric background $B(q)$ (see Fig. 3). To fit the data, we used $T_{max}=24.51\,^\circ$C and subtracted this scan from all the other data sets. We assumed that the error bars on each scan follow a Poisson distribution. The error bars for the left-hand side of Eq. (3) were obtained by adding the error bars from each individual scan in quadrature. We fit all the data sets simultaneously to Eq. (3) convolved to the detector resolution Δq.

Figure 3 shows the results of the fit to all the data for $20.01\leqslant T<25.35\,^\circ$C. The results for the three fit parameters varied were $T_c=19.12\,^\circ$C, $\xi_0=2.48$ Å, and $S(q=0)=4.86$ photons/s with a $\chi^2=1.83$. The measured data and fits for two extreme temperatures are shown, $T=20.01$ and $23.64\,^\circ$C. The fits are quite good. If one subtracts the critical component of the scattering found in the fit function, one can

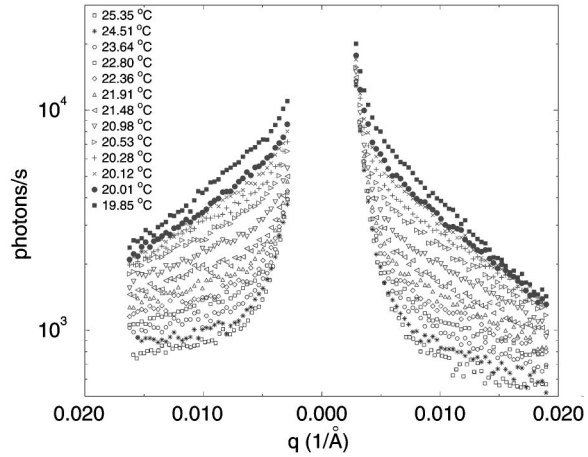

FIG. 2. The measured scattered intensity for the *n*-hexane–nitrobenzene mixture versus temperature. All scattering rates reported in this paper are normalized to an APS ring current of 100 mA.

test for the consistency of the approach. The dashed and dotted lines in Fig. 3 represent the maximum variability of the estimated background. The background for negative wave vector is constant over the temperature range but some variations are seen for positive wave vectors. The background is constant far away from T_c. Figure 3 also shows our estimate of the background with the sample in the beam. It was obtained by adding the measured background without any sample cell in the beam and the scattering rate from two 2 mil Kapton windows, and then scaling this sum by the measured transmission of the sample. The deduced background from the fits are higher than the estimated parasitic scattering from the beamline and windows. This is most likely caused by parasitic scattering from the sample cell itself which was not in the beam path in our measurement of the parasitic background.

Table III describes in more detail our fit parameter results. We fit all data sets with $T_{min} \leqslant T < T_{max}$ to Eq. (3), using

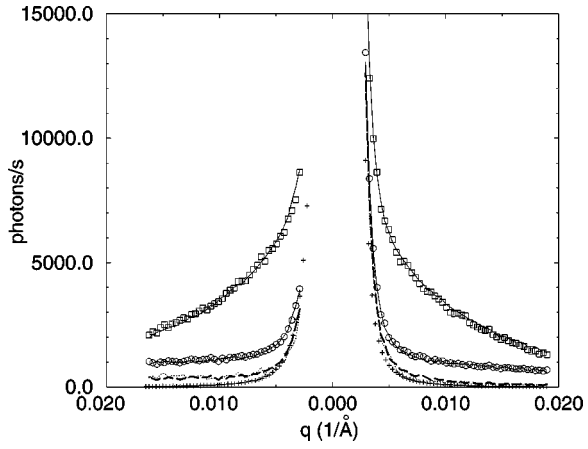

FIG. 3. The measured scattered intensity for two temperatures $T=20.01$ °C (squares) and $T=23.64$ °C (circles). The solid lines are fit to Eq. (3). The estimated backgrounds for $T=20.01$ °C (dotted line) and $T=23.64$ °C (dashed line) are shown as well as the best estimate of the parasitic scattering from the optics (+).

TABLE III. Results of fit parameters to Eq. (3).

T_{min} (°C)	χ^2	Sq_0 (photons/s)	ξ_0 (Å)	T_c (°C)
19.85	2.526	4.23±0.06	2.34±0.02	19.24±0.01
20.01	1.830	4.86±0.08	2.48±0.02	19.12±0.01
20.12	1.767	4.81±0.08	2.46±0.02	19.13±0.02
20.28	1.684	4.91±0.10	2.49±0.02	19.10±0.02

fixed critical exponents $\nu=0.635$ and $\gamma=1.23$. We found that by taking out the scan closest to T_c, $T=19.85$ °C, the χ^2 of the fits improved by 30 %. If this scan was included in the analysis, the fits would not converge to reasonable values, and the deduced background for positive wave vector would become negative. All type fits with $T_{min} > 19.85$ °C results in nearly identical fit parameters within error. For future discussion, we will use the results of the fit with $T_{min}=20.01$ °C.

We can now rescale the fitted model for concentration fluctuations to the absolute volume specific differential cross section given by

$$\frac{d\sigma_V}{d\Omega} = \frac{I(q,T)-B(q)}{\epsilon V I_i e^{-\Delta z/\delta}\Delta\Omega} = \frac{I(q,T)-B(q)}{\epsilon \Delta z F e^{-\Delta z/\delta}\Delta\Omega}, \tag{4}$$

where I_i is the incident x-ray intensity, $F=I_iA=7.7\times10^{10}$ photons/s is the total flux in the illuminated area A, $V=A\Delta z$ is the illuminated volume, $\Delta z=1.0$ cm is the sample thickness, $e^{-\Delta z/\delta}=0.34$ is the measured sample cell transmission, $\epsilon=0.82$ is the quantum efficiency, and $\Delta\Omega=(600\ \mu\text{m}/2.95\ \text{m})^2=4.13\times10^{-8}$ s is the detector solid angle. Using results of the fit for $T_{min}=20.01$ °C, the volume specific absolute differential cross section for concentration fluctuation in the mixture *n*-hexane–nitrobenzene is

$$\frac{d\sigma_V}{d\Omega} = \frac{5.47\times10^{-3}\ \text{cm}^{-1}t^{-\gamma}}{1+q^2\xi_0^2 t^{-2\nu}}. \tag{5}$$

It is often important to predict the scattering rate from a binary mixture in order to find the materials that have the highest cross section. One can show that the absolute cross section from a binary mixture can be written approximately as

$$\frac{d\sigma_V}{d\Omega} = r_e^2(\Delta\rho_e)^2 k_B T \chi G(q\xi), \tag{6}$$

where $r_e=2.8\times10^{-15}$ m is the classical electron radius, $(\Delta\rho_e)=144e/\text{nm}^3$ is the electron density difference between the mixture's components (see Table I). If one assumes that the compressibility can be approximated by the osmotic compressibility of an ideal gas mixture, χ, with a critical multiplying factor (this is valid for hexane-nitrobenzene within a factor 2 using light scattering results), then $\chi = t^{-\gamma}c(1-c)\langle v_0\rangle/(k_BT)$. Here c is the concentration in mole fraction and $\langle v_0\rangle$ is the average molecular volume. Then Eq. (6) can be rewritten as

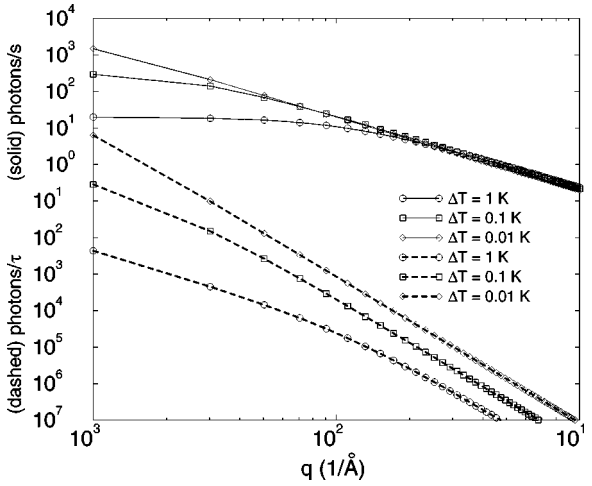

FIG. 4. The predicted scattering rates per speckle for *n*-hexane and nitrobenzene for coherent conditions (solid line) for different $\Delta T = T - T_c$. The scattering rate per speckle per correlation time (dashed line). The symbols here help to distinguish the different predictions.

$$\frac{d\sigma_V}{d\Omega} \approx r_e^2 (\Delta\rho_e)^2 c(1-c)\langle v_0\rangle t^{-\gamma} G(q\xi)$$

$$\approx k^* t^{-\gamma} G(q\xi). \tag{7}$$

Note that for strong scattering from a binary system, it is important to have a large electron density difference between the components and a small average electron density for a large x-ray penetration depth. This is the case for hexane-nitrobenzene mixtures. Using $c = 0.416$ for the critical composition of nitrobenzene, and $\langle v_0\rangle = 0.194$ nm^3 for the average molecular volume, the prefactor in Eq. (7) is $k^* = 7.66 \times 10^{-2}$ cm^{-1}, which is a factor 14 more than the measured factor for the cross section in Eq. (5). Although the predicted intensity is overestimated, we have found Eq. (7) helpful to select a strongly scattering system. Note that if one transforms estimates of the absolute cross section derived for neutron scattering to x-ray scattering using relationships derived in the work of Schneider *et al.* [21], transforming neutron scattering lengths to x-ray scattering lengths, i.e., (Zr_e), one finds that the theoretical estimate becomes a factor 16 larger than measured. Thus, Eq. (7) agrees well with estimates of the cross section derived from neutron scattering. It is not clear why this difference remains.

We next discuss the feasibility of an XPCS experiment on this mixture. If we set a coherent aperture of 5 μm $\times 5$ μm in front of the sample, we will lose a factor $(100/5)^2 = 400$ in signal compared to Fig. 2. Similarly in an XPCS experiment with a 5 μm$\times 5$ μm beam, one must close the slits A4 to limit the detector area to a speckle area. The speckle size is of order $\lambda R_d/a$, where R_d is the sample-detector distance and a is the aperture size. At 2.95 m and 11 keV, the speckle size is thus 67 μm. This will further reduce the scattering rate by a factor $(600/67)^2 = 80$. Figure 4 shows the predicted coherent scattered intensity per speckle as a function of q and ΔT. We have also assumed a conservative gain of a factor 100 in incident flux due to the use of a pink beam.

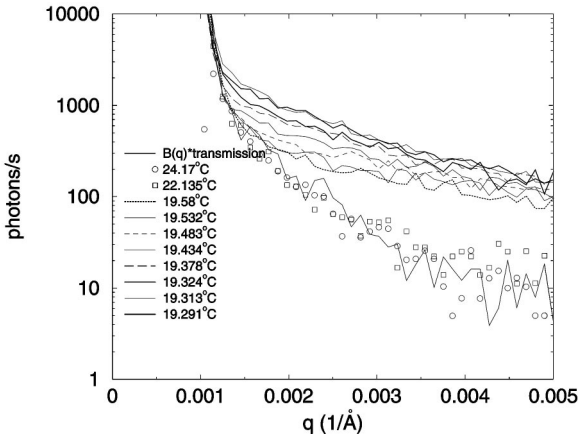

FIG. 5. The scattered intensity vs the wave vector q for several temperatures in a $(20\ \mu\text{m})^2$ detector area.

The real figure of merit for a PCS experiment is the count rate per speckle per correlation time. For simplicity, we estimate the correlation time with the Stokes-Einstein relation

$$\tau = 6\pi\eta\xi/(k_B T q^2), \tag{8}$$

where η is the shear viscosity. The shear viscosity of the *n*-hexane–nitrobenzene mixture is 0.0053 P [14]. The correlation time can be conveniently written as $\tau = 4.67 \times 10^{-10}\eta[\text{P}]\xi[\text{Å}]/q^2[\text{Å}^{-2}]$. The correlation time of the fluctuations 0.1 °C away from T_c for a wave vector of 0.004 Å^{-1} is 61 μs, which can be sampled with a standard hardware correlator. In Fig. 4, the product of the calculated correlation time, τ, with the predicted count rate per speckle is also shown. Thus with an improvement in x-ray optics by using a pink beam, providing an increase in coherent flux of a factor 100 over the current setup, it is possible to obtain accurate decay rates 0.1 °C away from T_c.

B. XPCS results

Figure 5 shows the temperature dependence of the scattered intensity for the mixture of *n*-hexane and nitrobenzene normalized to a constant incident coherent intensity of 3.6×10^{10} photons/s in an aperture of $(5\ \mu\text{m})^2$. The incident intensity with the pink beam was a factor 187 larger than with the monochromatic beam, but the sample thickness was reduced by a factor 10/3. The background measured without a sample and scaled for the transmission of the sample (29.5%) is shown in Fig. 5. For all data, the background is smaller than the scattered intensity for $q > 0.005$ Å^{-1}. Closer to the main beam, the background becomes a larger fraction of the total scattered intensity. The intensity saturates at 19.313 °C, and the data at $T = 19.291$ °C are below T_c. Thus we estimate that the critical temperature is $T_c \approx 19.30$ °C. This measurement is slightly different from our SAXS results (≈ 19.12 °C), likely because the sample cell was redesigned for the XPCS measurement to improve the temperature stability. With this new oven, the sample was

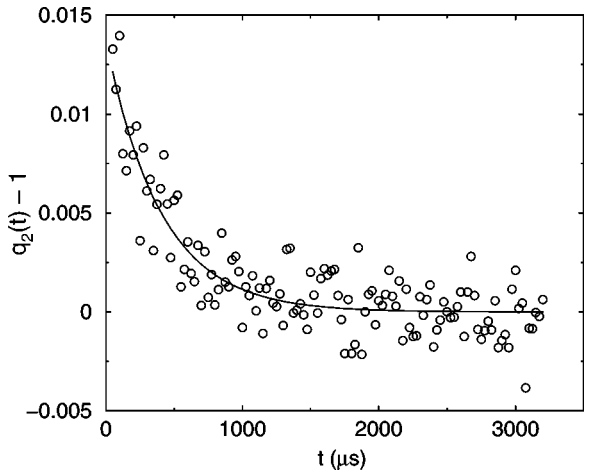

FIG. 6. The measured correlation function versus the delay time at $q = 0.001\,56$ Å^{-1} and $T = 19.363\,^{\circ}$C. The solid line is an exponential least squares fit described in the text.

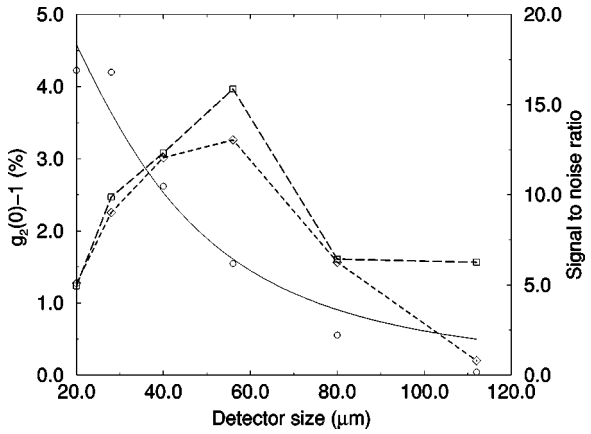

FIG. 7. The contrast versus the detector aperture (left axis, circles). The solid line is a fit as discussed in the text. The signal to noise ratio calculated from the data versus the detector aperture is also shown (right axis, squares). The dashed line is a guide to the eye. The calculated SNR from Eq. (11) (diamonds).

more shielded from the warm surroundings and the thermistor was closer to the sample than in the first design. The excellent temperature stability achieved was essential in this measurement.

Figure 6 shows the dynamic correlation function of the scattered intensity versus the delay time of the correlator at $q = 0.001\,56$ Å^{-1}, and $T = 19.363\,^{\circ}$C. The detector aperture A4 was set to 58 μm$\times$58 μm to optimize the signal to noise ratio of our data collection (see below). The sampling time was 25 μs, and typical collection times were on the order 30–60 min (see Table IV). The data for the first delay time are affected by dead time, thus it is removed from Fig. 6. The correlation function was fit to

$$g_2(t) - 1 = \frac{\langle I(q,t) I(q,0) \rangle}{\langle I \rangle^2} - 1 = \beta \exp(-2t/\tau), \qquad (9)$$

where $\beta = 0.0137$ is the contrast and $\tau = 805$ μs the relaxation time of composition fluctuations of the mixture.

Figure 7 shows the contrast, β, and signal to noise ratio, SNR, as a function of detector aperture size. The SNR was calculated from the data by the ratio of the fitted β, divided by the rms noise at long time delay estimated over several adjacent correlator channels (squares). The results shown in Fig. 7 are representative of the dependence on detector size, but the vertical scale is somewhat sensitive to the amount of parasitic scattering collected, which depends upon wave vector, among other things, and generally increases with decreasing wave vector. With a detector aperture of (20 μm)^2, we measured a contrast as high as 8%, although we typically opened the detector aperture to improve the SNR of g_2.

A simple model [17] for the dependence of the contrast on detector aperture due to spatial averaging of the speckles is given by

$$\beta = \frac{\beta_o}{1 + A/A_s}, \qquad (10)$$

where β_o is the contrast in the limit of zero detector size (i.e., no spatial averaging), A is the detector area, and A_s is the speckle area. A fit of this equation to the contrast measurements is shown in Fig. 7 as the solid line. The deduced speckle size is 33 μm and β_o is 6.3%. The deduced speckle size is somewhat larger than the 20 μm we estimated based on our aperture size. However, the data with detector size $>$ 25 μm were collected with sample times of 25 μs whereas data with detector size $<$25 μm were collected with sample times of 50 μs due to their lower SNR. Thus there may be some additional reduction in β in Fig. 7 due to time averaging of the 350 μs relaxations for smaller detector apertures

TABLE IV. Fit parameters at $T = 19.363\,^{\circ}$C for the mixture *n*-hexane and nitrobenzene. β is the contrast, and σ is the standard deviation of the correlation function, thus β/σ is the S/N ratio of our measurement. The ratio of the background $B(q)$ over the total intensity $I(q)$ is also shown.

q (Å^{-1})	$\langle I \rangle$ (photons/s)	Collection time (s)	τ (μs)	β (%)	β/σ	$B(q)/I(q)$
0.00120	12852	1195	2135.5	0.274	5.6	
0.00156	4567	1079	804.7	1.37	11.3	0.56
0.00209	2339	1990	379.6	1.57	8.2	0.24
0.00209	2031	2164	366.1	1.19	5.5	0.24
0.00261	1475	3822	252.0	1.93	6.8	0.16
0.00261	1509	5144	283.5	1.07	6.05	0.16

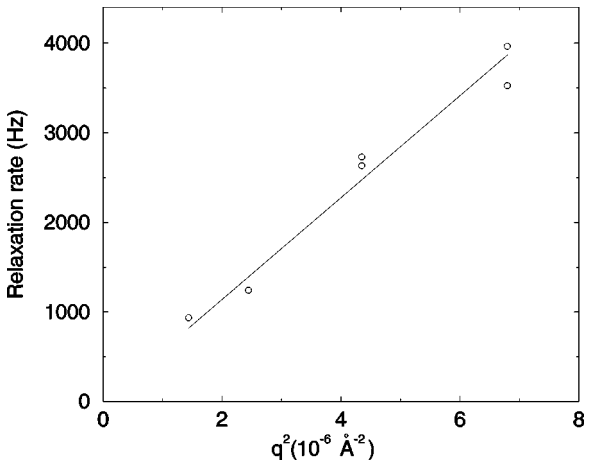

FIG. 8. The relaxation rate $(1/\tau)$ versus the square of the wave vector. The solid line is a linear least squares fit to the data.

which is not present for larger apertures. Nevertheless, a simple model of spatial averaging explains the data quite well.

The dependence of SNR shown in Fig. 7 is also easily understood. For small detector apertures, the increasing rms noise reduces the SNR since the measurements were all for the same total time duration. At larger detector apertures, spatial averaging of the speckles reduces the SNR. We find a maximum in the SNR for a detector aperture which is ≈ 2 to 3 times the speckle size, as expected based on experience with visible light PCS.

In Fig. 7, we also plot the SNR from a calculation presented in Appendix A of Ref. [8]. One can show that the signal to noise ratio $\mathcal{R}_{\mathrm{S.N}}$ in the limit of small count rate follows

$$\mathcal{R}_{\mathrm{S.N}} = \beta \langle I \rangle \sqrt{\frac{T\Delta t}{1+\beta}}, \tag{11}$$

where $\langle I \rangle$ is the average count rate, T the experiment duration, and Δt, the sampling time. Both calculated data sets have a peak at the same detector slit opening of 56 μm. Eq. 11 is quite convenient to determine an experimental procedure for efficient data collection.

Table IV shows the fitted parameters for several wave vectors at the same fixed temperature. For two wave vectors, the data was repeated twice. The correlation time was overall quite reproducible given that the data collection was reproduced several hours after it was first taken. This consistency also shows that the sample was not easily radiation damaged. In fact, none of our observations indicated that the sample was affected by the x-ray beam. As noted in the Introduction, this tolerance to high intensity x-ray beam is remarkable among soft condensed matter, organic systems, such as colloids or polymers, which are generally much more susceptible to radiation induced charging or damage effects. In this case, we speculate that the low viscosity of the mixture and concomitant high diffusion coefficient contribute to alleviating the effects of any radiation damage that may occur.

Figure 8 shows the relaxation rate versus the square of the wave vector for the critical mixture at $T = 19.363\,^{\circ}\mathrm{C}$. In Table IV, we noticed that the correlation time for the smallest wave vector was much larger than expected. The signal to noise ratio of the correlation function is small at this wave vector and the intercept at zero delay time of g_2 is much smaller than expected. For a wave vector so close to the main beam, we believe that the stray parasitic background $B(q)$ reduces the contrast and signal to noise of ratio g_2. Furthermore, we believe that the scattered field from the sample is heterodyning with the main beam which acts as a reference signal. When such a phenomena occurs, it is well known that the measured contrast and S/N ratio of the correlation function is reduced, and the correlation time is twice as long as in a homodyne measurement. In Fig. 8, we have thus divided the correlation time of the smallest wave vector measured by a factor 2. The solid line is a fit to $1/\tau = Dq^2$ with a diffusion constant $D = 5.69 \times 10^8$ Å^2/s. The data clearly shows simple diffusive relaxation for the range of wave vectors shown.

Using our SAXS measurements, one estimates the correlation length in Fig. 8 as $\xi = \xi_0 t^{-0.635} = 524$ Å, with $\xi_0 = 2.46$ Å. From Eq. (8), the diffusion constant is $D = k_B T/6\pi\eta\xi$. Replacing for the known viscosity, the Stokes-Einstein relation results in an estimate of $D = 7.71 \times 10^8$ Å/s, which is in fairly good agreement with our estimate of D from the slope of Fig. 8.

Previous light scattering results of the relaxation rate of *n*-hexane–nitrobenzene use a mode coupling theory to explain the complete wave vector dependence of the relaxation rate [14]. In these theories, the normalized critical relaxation rate $\Gamma^* = 6\pi\eta\Gamma/(k_B T q^3)$ versus $x = q\xi$ follows a Kawasaki-Low approximation. For small $x \ll 1$ in the hydrodynamics regime, $\Gamma^* \propto 1/x$, while in the critical regime for $x \gg 1$, the normalized relaxation rate is constant. The crossover region is around $x = 1$. Result obtained by Chen *et al.* ranged in x from 0.006 to 51 [14]. They were able to distinguish subtle effects where more complicated theories including a non-critical background relaxation rate needed to be included with the critical component to explain the data over the full range of x. Such large x were accessible because they reached within 3 mK of the critical point. We probed the crossover region up to $x = 1.4$ in this study. To probe larger x than light scattering measurements could reach, one will have to get much closer to T_c than we have, and probe higher wave vectors. It is possible that our critical data were affected by temperature gradients generated by the pink beam. Back of the envelope calculations derived in Appendix B show that temperature differences on the illuminated volume are of the order of 8 mK for a small pink beam. Also the center of the illuminated area could be 97 mK warmer than the sample holder. Future studies should consider reducing the incident flux by making the bandwidth a factor 10 smaller and improving detector collection efficiency though the use of parallel detection with a fast CCD detector.

In summary, we have performed a SAXS study of the binary mixture *n*-hexane–nitrobenzene near its critical point. We extracted the critical component of the measured scattered intensity from the data by fitting the data to a scaling form. Within the accuracy of the data, the critical exponents

observed are consistent with previous light scattering measurements. We reported the absolute x-ray scattering cross section of the mixture and compared it to an approximate theoretical expression. This approach is helpful in determining good candidates for XPCS.

We performed XPCS on the mixture at a fixed temperature of about 63 mK above the critical point. With a pink beam providing an additional two decades of coherent flux over our monochromatic SAXS measurements, we were able to measure a scattered intensity of several hundred counts/s per speckle above the critical point. Although this mixture is composed of low molecular weight hydrocarbons, it has a large x-ray contrast and x-ray penetration depth, which makes it a good scatterer for XPCS. Using a hardware correlator we were able to measure the XPCS dynamic correlation function on a simple binary fluid. Although rather fast (250 μs), we were able to measure the correlation functions with sufficient signal to noise ratio within an hour of collection time. This x-ray PCS measurement would not have been possible without the large coherent flux provided by a third generation source such as the Advanced Photon Source. The diffusion constant deduced from the XPCS measurement is consistent with the estimates from light scattering measurements.

These measurements demonstrate the feasibility of using XPCS to study the dynamics of even such weak scatterers as these low molecular weight hydrocarbon fluid mixtures. This further demonstrates the general applicability of XPCS to a wide variety of materials. We found no detectable signs of radiation damage in these mixtures even under the high intensity of a pink undulator beam at a third generation source such as the APS. We believe that other fluid mixtures should also scatter sufficiently to study critical dynamics in a new range of large wave vectors previously inaccessible. Studies of binary fluids in confined geometries should also benefit from this technique.

ACKNOWLEDGMENTS

We are grateful for the support and assistance of Harold Gibson, Try Leng Kruy, Thomas Sanchez, Ernest Williams, and Walter Lowe. We acknowledge support under NSF Grant No. DMR 92-14220, DOE Grant Nos. DE-FG02-94ER45513 and DE-FG02-99ER45743, and the donors of the Petroleum Research Fund, administered by the American Chemical Society under Grant ACS-PRF No. 32105-AC7. Use of the Advanced Photon Source was supported by the U.S. Department of Energy, Basic Energy Sciences, Office of Energy Research, under Contract No. W-31-109-ENG-38.

APPENDIX A: COHERENT CONDITIONS

It is well known that the longitudinal coherent condition will be satisfied for small scattering angles 2θ such that the largest path difference in the sample $D2\theta + t\theta^2/2 < l_l$, where $D=5$ μm is the beam size, $t=3$ mm is the sample thickness, and $\theta \ll 1$. Here the second quadratic term is negligible and the limiting angle $\theta = 0.5 l_l / D = 0.18$ mrad. This scattering angle yields a limiting wave vector $q = 4\pi/\lambda\theta < 1.6 \times 10^{-3}$ Å^{-1}.

Given that the sample sits about 26 cm from the coherence limiting slit A2, the beam diffracts out, thus the beam size on the sample which defines the speckle size in the detector plane is larger than 5 μm. The beam size on the sample is approximately $D_s = \sqrt{D^2 + \lambda^2 R_c^2 / D^2}$, where $R_c = 0.263$ m is the coherence slit-sample distance, and $D = 5$ μm the opening of aperture A2. One finds that $D_s = 8.8$ μm. The speckle size in the detector plane will thus be $\lambda R_d / D_s = 20$ μm, with a sample to detector distance $R_d = 1.24$ m.

APPENDIX B: ESTIMATES OF THERMAL GRADIENTS

We estimate the thermal profile induced by the beam assuming the following boundary conditions: a cylindrical sample with radius r_1 and thickness Δz, illuminated by a circular x-ray beam of radius $r_0 < r_1$. The cooling block has a fixed temperature $T(r=r_1) = T_1$. Assuming that the heat is absorbed uniformly throughout the sample thickness, one can solve the two-dimension heat equation and show that largest temperature difference is $\Delta T_{max} = T(0) - T(r_1) = P/(2\pi\kappa\Delta z) * [\ln(r_1/r_0) + 0.5]$, where κ is the heat conductivity, and P the absorbed power in the sample. One can also show that the temperature difference between the center and edge of the beam $\Delta T_{beam} = T(0) - T(r_0) = P/(4\pi\kappa\Delta z)$. For the hexane-nitrobenzene mixture we further approximate the thermal conductivity of the mixture to be that of pure hexane with $\kappa = 0.123$ mW/(K mm). The pink beam power is $P = 50.3$ μW and the measured absorption factor was 70.5%. The sample diameter was 3.5 mm, the thickness was 3 mm, and we assume that the beam was circular with a radius $r_0 = 5$ μm such that $\pi r_0^2 = D_s^2$. Replacing these values, one finds $\Delta T_{beam} = 7.6$ mK, $\Delta T_{max} = 97$ mK.

[1] S. Brauer, G. Stephenson, M. Sutton, R. Brüning, E. Dufresne, S. Mochrie, G. Grübel, J. Als-Nielsen, and D. Abernathy, Phys. Rev. Lett. **74**, 2010 (1995).

[2] S. Dierker, R. Pindak, R. Fleming, I. Robinson, and L. Berman, Phys. Rev. Lett. **75**, 449 (1995).

[3] T. Thurn-Albrecht, W. Steffen, A. Patkowski, G. Meier, E. Fischer, G. Grübel, and D. Abernathy, Phys. Rev. Lett. **77**, 5437 (1996).

[4] J. Mainville, F. Bley, F. Livet, E. Geissler, J. Legrand, D. Abernathy, G. Grübel, S. Mochrie, and M. Sutton, J. Appl. Crystallogr. **30**, 828 (1997).

[5] S. Mochrie, A. Mayes, A. Sandy, M. Sutton, S. Brauer, G. Stephenson, D. Abernathy, and G. Grübel, Phys. Rev. Lett. **78**, 1275 (1997).

[6] O. Tsui and S. Mochrie, Phys. Rev. E **57**, 2030 (1998).

[7] A. Poniewierski, R. Holyst, A. Price, L. Sorensen, S. Kevan, and J. Toner, Phys. Rev. E **58**, 2027 (1998).

[8] T. Thurn-Albrecht, G. Meier, P. Müller-Buschbaum, A.

Patkowski, W. Steffen, G. Grübel, D. Abernathy, O. Diat, M. Winter, M. Koch, and M. Reetz, Phys. Rev. E **59**, 642 (1999).
[9] L. Lurio, D. Lumma, A.R. Sandy, M. Borthwick, P. Falus, S. Mochrie, J. Pelletier, M. Sutton, L. Regan, A. Malik, and G. Stephenson, Phys. Rev. Lett. **84**, 785 (2000).
[10] M. Sutton, S. Mochrie, T. Greytak, S. Nagler, L. Berman, G. Held, and G. Stephenson, Nature (London) **352**, 608 (1991).
[11] B. Chu, *Laser Light Scattering: Basic Principles and Practice*, 2nd ed. (Academic Press, Boston, 1991).
[12] A. Malik, A. Sandy, L. Lurio, G. Stephenson, S. Mochrie, I. McNulty, and M. Sutton, Phys. Rev. Lett. **81**, 5832 (1998).
[13] E. Dufresne, Ph.D. thesis, McGill University, 1995.
[14] S.-H. Chen, C.-C. Lai, J. Rouch, and P. Tartaglia, Phys. Rev. A **27**, 1086 (1983).
[15] P. Damay, F. Leclercq, and P. Chieux, Phys. Rev. B **40**, 4696 (1989).
[16] Y. Izumi, Phys. Rev. A **39**, 5826 (1989).
[17] J. Goodman, *Statistical Optics*, 1st ed. (Wiley, New York, 1985), pp. 465–532.
[18] A. Sandy, L. Lurio, S. Mochrie, A. Malik, G. Stephenson, J. Pelletier, and M. Sutton, J. Synchrotron Radiat. **6**, 1174 (1999).
[19] P. Ilinski, R.J. Dejus, E. Gluskin, and T.I. Morrison, in *Optics for High-Brightness Synchrotron Radiation Beamlines II* (SPIE, The International Society for Optical Engineering, Bellingham, WA, 1996), Vol. 2856, pp. 16–25.
[20] T. Nurushev, Ph.D. thesis, University of Michigan, 2000.
[21] R. Schneider, L. Belkoura, J. Schelten, D. Woermann, and B. Chu, Phys. Rev. B **22**, 5507 (1979).